Sensors & Actuators: B. Chemical 462 (2026) 140001

Contents lists available at ScienceDirect

Sensors and Actuators: B. Chemical

journal homepage: www.elsevier.com/locate/snb

Overcoming dynamic-range limitations in dual-gas sensing via dual-mode QTF excitation

Xiaowen Shen [a,b,c], Chaofeng Sun [a,b], Pietro Patimisco [c], Angelo Sampaolo [c], Vincenzo Spagnolo [c,*], Lei Dong [a,b,**], Hongpeng Wu [a,b,**]

[a] State Key Laboratory of Quantum Optics Technologies and Devices, Institute of Laser Spectroscopy, Shanxi University, Taiyuan 030006, PR China
[b] Collaborative Innovation Center of Extreme Optics, Shanxi University, Taiyuan 030006, PR China
[c] PolySense Lab-Dipartimento Interateneo di Fisica, University and Politecnico of Bari, Via Amendola 173, Bari, Italy

ARTICLE INFO

Keywords:
Dual-spectral
Multi-gas detection
LITES
QEPAS

ABSTRACT

Simultaneous detection of multiple gases with concentrations spanning five to six orders of magnitude remains a significant challenge for conventional sensing technologies. In this work, we present a dual-spectral (QEPAS-LITES) multi-gas detection system based on a single customized quartz tuning fork (QTF). By applying second-harmonic (*2 f*) wavelength modulation at 1368.6 nm and 1653.7 nm, the fundamental and first-overtone resonance modes of the QTF are excited concurrently, enabling intrinsic frequency-domain separation and parallel demodulation of photoacoustic and photothermal signals. This streamlined architecture enables truly simultaneous monitoring of percent-level H_2O and ppm-level CH_4, effectively overcoming the dynamic-range limitations of standard multi-gas sensing. Excellent linearity is obtained for both species ($R^2 = 0.9999$ for H_2O and 0.998 for CH_4), with minimum detection limits of approximately 30 ppm and 660 ppb, respectively. Allan-Werle deviation analysis confirms stable long-term operation for both detection channels. By overcoming the dynamic-range and saturation limitations of conventional multi-gas sensors, the proposed dual-mode approach provides a robust and scalable platform for wide-dynamic-range gas sensing in applications including atmospheric greenhouse gas monitoring, industrial emission analysis, and complex open-path environments.

1. Introduction

Online multi-component gas detection plays a crucial role in a wide range of fields, including environmental greenhouse gas monitoring, industrial process safety, and biomedical breath analysis [1–5]. A major challenge arises when target species coexist at concentrations differing vastly different concentrations, often spanning five to six orders of magnitude. For example, atmospheric monitoring requires detecting trace methane (CH_4, at ~1.9 ppm) in the presence of abundant water vapor (H_2O, at 1%–5%), while industrial emission analysis may involve simultaneous measurement of ppb-level pollutants (e.g., NO_x) alongside percent-level CO_2. Such scenarios impose stringent requirements for sensing technologies: high sensitivity for trace components, strong resistance to saturation for dominant species, robust, interference-free discrimination of multi-species signals. Nevertheless, conventional gas-sensing techniques face fundamental limitations in meeting these demands. Electrochemical sensors, though compact and low-cost, exhibit poor selectivity, substantial cross-interference (e.g., H_2O affecting CH_4 readings), and limited operational lifetimes [6–7]. Semiconductor sensors offer fast response times but are susceptible to environmental fluctuations and lack molecular specificity [8–9]. Among optical methods, tunable diode laser absorption spectroscopy (TDLAS) provides excellent selectivity, yet their dynamic range is constrained (~3–4 orders of magnitude) and signal saturate at high concentrations [10–13]. Cavity-enhanced methods, including cavity ring-down spectroscopy (CRDS) [14] and cavity-enhanced absorption spectroscopy (CEAS) [15] achieve outstanding sensitivity (down to ppb-level) but rely on enclosed high-finesse cavities, which hinder sensing applications and are prone to mirror contamination. Conventional photoacoustic spectroscopy (PAS) [16–21] offers strong immunity to optical interference but depends on bulky acoustic microphones and direct gas-sensor contact, rendering it unsuitable for corrosive or open-path environments.

* Corresponding author.
** Corresponding authors at: State Key Laboratory of Quantum Optics Technologies and Devices, Institute of Laser Spectroscopy, Shanxi University, Taiyuan 030006, PR China.
E-mail addresses: vincenzoluigi.spagnolo@poliba.it (V. Spagnolo), donglei@sxu.edu.cn (L. Dong), wuhp@sxu.edu.cn (H. Wu).

https://doi.org/10.1016/j.snb.2026.140001
Received 3 February 2026; Received in revised form 3 April 2026; Accepted 16 April 2026
Available online 17 April 2026
0925-4005/© 2026 Elsevier B.V. All rights are reserved, including those for text and data mining, AI training, and similar technologies.

Quartz-enhanced photoacoustic spectroscopy (QEPAS) overcomes several limitations of conventional photoacoustic methods by employing a miniaturized quartz tuning fork (QTF, typically ~5 ×3 ×0.25 mm^3) as a high-Q acoustic detector, enabling compact, robust, and selective gas detection across multiple species [22–30]. However, standard QEPAS architectures are primarily designed for gas mixtures with relatively narrow concentration ranges (ppm-percent). Their performance degrades substantially in scenarios where trace gases coexist with highly abundant components. Strong photoacoustic signals generated by dominant species can saturate the QTF response, masking weak signals from trace analytes and compromising quantitative accuracy. Additionally, cross-sensitivity and spectral overlap hinder reliable multi-species discrimination under high dynamic-range conditions. A further limitation arises from the contact-based nature of QEPAS direct exposure of the QTF to corrosive gases such as NO_x, H_2S or SO_2 can lead to electrode degradation, frequency drift, reduced quality factor, and ultimately sensor failure [31–32]. The intrinsic need for physical interaction with the gas sample restricts the use of QEPAS in applications requiring remote sensing capability or operation in chemically aggressive or strongly concentration-stratified environments. To mitigate these drawbacks, laser-induced thermoelastic spectroscopy (LITES) was introduced [33–36]. Based on the detection of laser-induced thermoelastic waves in solids, LITES eliminates the need for mechanical resonators and enables rapid response, high mechanical robustness, and inherent remote-sensing capability. However, its sensitivity to trace gases is generally lower than that of QEPAS due to inherent thermoelastic signal attenuation.

To leverage the high sensitivity of QEPAS together with the sensing and robustness advantages of LITES, several hybrid configurations have been investigated. In 2021, Hu et al. [37] proposed a dual-QTF configuration (QEPAS-PTS) capable of generating both photoacoustic and photothermal signals; however, the system remained restricted to single-gas detection and suffered from intrinsic frequency mismatch between the two tuning forks. Qiao et al. [38] later introduced a single-QTF dual-signal (S-QEDS) scheme that eliminated the mismatch issue, but its functionality was still limited to one target species. In 2023, Cui et al. [39] presented a multi-pass cell (MPC) enhanced dual-spectroscopy method that increased the C_2H_2 signal by nearly 80-fold, yet the persistent problem of crosstalk between photoacoustic and photothermal channels remained unsolved. Most recently, Liang et al. [40] developed a QEPAS-LITES hybrid sensor for dissolved-gas monitoring in deep-sea environments. Although their system improved stability for CH_4, CO_2, H_2S, and NH_3 by using LITES as an auxiliary correction for QEPAS, it neither enabled true simultaneous multi-species detection nor supported open-path operation, as it relied on closed measurement cell.

In this work, we present an integrated dual-mode QEPAS-LITES platform utilizing a single customized quartz tuning fork (QTF) to overcome the dynamic-range limitations of conventional sensors. By concurrently exciting the fundamental and first-overtone resonance modes of the QTF, the system achieves intrinsic frequency-domain isolation, enabling the parallel, crosstalk-free demodulation of photoacoustic and photothermal signals. This unique architecture effectively bypasses signal saturation in high contrast gas mixtures, allowing for the truly simultaneous detection of percent-level H_2O and ppm-level CH_4. Compared to multi-sensor configurations, our approach significantly streamlines the optical layout and calibration complexity. We demonstrate a robust, scalable platform that provides a superior solution for wide dynamic range, multi-species monitoring in complex and concentration stratified gas environments.

2. QTF Fundamental mode and overtone mode theoretical background

To ensure effective excitation and detection of gas signals, the modulation frequency of the optical excitation must remain much lower than the molecular relaxation rate of the target species. This requirement imposes a constraint on the acoustic sensor: the resonance frequency of the QTF must satisfy $f \ll 1/(2\pi\tau)$, where τ is the relaxation time. In practice, QTF operating above ~50 kHz fail to meet this condition for many slow-relaxing gas molecules. Standard commercial quartz tuning forks, however, have a fundamental resonance frequency of approximately 32.76 kHz, a quality factor (Q value) of around 10000, while their first overtone mode lies above 190 kHz [41]. Consequently, the high-order modes of conventional QTFs are unsuitable for QEPAS operation because they violate the relaxation-frequency constraint and cannot be efficiently driven by wavelength-modulated photoacoustic excitation. To overcome this limitation, we employed a customized QTF specifically designed with substantially lower resonance frequencies. This device exhibits fundamental and overtone modes in the few-kHz to tens-of-kHz range [42], characterized by its larger dimensions and lower resonance frequencies compared to standard QTFs, was intentionally selected to optimize the excitation of both the fundamental and the first-overtone modes. This design ensures that both modes possess high Q-factors and a wide frequency spacing, providing the necessary frequency-domain orthogonality required for the simultaneous, crosstalk-free detection of gases with vastly different concentration levels. Structurally, the custom QTF is approximately 4.6 times larger than a standard 32-kHz fork and features a high aspect ratio of 17:1. Specifically, this custom design has a prong length (L) of 17 mm and a prong thickness (T) of 1 mm. Additionally, it features a crystal width (w) of 0.25 mm and a prong spacing of 0.7 mm. The resonance frequency f_n of the nth vibration mode of the QTF can be expressed as

$$f_n = K \times \frac{T}{L^2} \times n^2$$

where K is a material-dependent constant (determined by quartz density and Young's modulus), T is the prong-tip width, and L is the prong length. Numerical analysis shows that $n = 1.194$ corresponds to the fundamental mode, whereas $n = 2.988$ represents the first overtone mode of the customized fork.

Previous studies [24–25] successfully simulated both the fundamental and the 1st overtone vibration modes of the customized quartz tuning fork, demonstrating that a multi-gas sensor based on frequency-division multiplexing can simultaneously exploit these two resonances to detect different gas species with high stability and sensitivity. Building on this foundation, we propose a dual-mode approach that assigns the fundamental resonance to photoacoustic detection and the first overtone to photothermal detection. In the proposed configuration, one modulated laser beam is focused in the gap between the tuning fork prongs near to their top to generate a photoacoustic response. A second modulated laser beam is directed onto the uncoated quartz crystal region at the base of the tuning fork vibrating arms, inducing a thermoelastic photothermal response.

Fig. 1 illustrates a possible scheme for the proposed dual-mode detection scheme. In Fig. 1(a), the simulated vibrational pattern shows the simultaneous excitation of the fundamental and the 1st overtone modes, which are responsible for generating the photoacoustic and photothermal signals, respectively. Fig. 1(b) depicts the combined vibration state produced when two independently modulated laser beams are incident at their designated excitation positions, depicting how both modes can be concurrently driven without mutual interference.

3. Description of the sensor system

3.1. Schematic diagram of the sensor

Fig. 2 presents the main modules of the dual-spectral multi-gas detection system, which utilizes a single customized quartz tuning fork (QTF) with a fork 17-mm prong length as the unified signal receiver. The setup consists of two functional subsystems, i.e., a QEPAS and a LITES

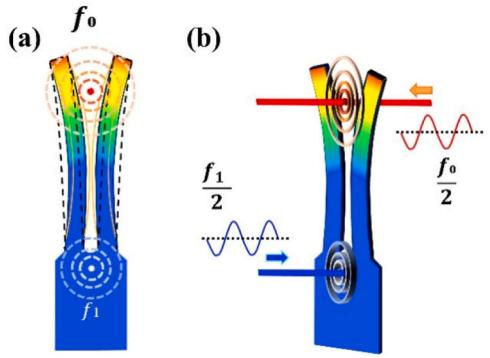

Fig. 1. (a) Simulated displacement field showing the combined excitation of the fundamental and first-overtone vibration modes; (b) Simulated response of the QTF when two independently modulated laser beams are simultaneously incident at the designated excitation points, illustrating the generation of the combined vibration state.

modules. In the QEPAS section, a DFB laser (Laser 1, L1) mounted on a temperature- and current-controlled driver board (Driver 1, D1) delivers the excitation beam. After collimation, the beam is directed between the QTF prongs and excites either the fundamental or first-overtone mode to generate the corresponding photoacoustic signal. The customized QTF is housed inside a gas chamber equipped with two CaF_2 windows for optical access. Despite minor Fresnel reflection losses at the interfaces, these windows maintain a high transmittance of over 93.5% in the near-infrared region, guaranteeing sufficient optical power delivery with negligible impact on measurement accuracy. The chamber inlet is connected to a controlled H_2O:N_2 gas mixture, regulated via a mass-flow controller (Alicat M-500SCCM-D) and a needle valve. At the outlet, a vacuum pump (KNF Technologies Ltd., N816.3KT.18) maintains the desired flow rate and chamber pressure, ensuring stable operating conditions.

For the LITES module, a second DFB laser (Laser 2, L2), controlled by a stabilized driver (Driver 2, D2), serves as the excitation source. The laser beam passes through a modular gas interface, currently configured with a 15-cm absorption cell (capable of integrating a multipass cell or other cell types for scalable sensitivity). The beam is then focused by a 50-mm focal-length lens onto the quartz tuning fork surface. Remarkably, the entire detection system fits within a volume of ~ $25 \times 6 \times 8$ cm^3. This highly integrated design drastically reduces the sensor's physical footprint relative to conventional QEPAS/LITES setups, facilitating deployment in space-constrained environments.

Fig. 3 illustrates the selected lasers focusing positions for photoacoustic and photothermal excitations. Previous experiments have shown that the strongest QEPAS response for the fundamental mode occurs when the laser beam is focused near the upper region of the QTF [42]. The same experiments demonstrate that the overtone mode shows two antinode positions, one located 9.5 mm from the QTF top and another one located near the QTF top. Since there is no big difference in terms of signal intensity between these two antinode positions, to avoid adjustments of the laser alignment when changing detection channels, we prefer to fix the laser focusing position for QEPAS (L1) at 2.0 mm from the prong tip.

Thereby, 1368.6 nm beam (L1) has been focused between the QTF prongs near the upper region of the fork, approximately 2.0 mm from the prong tip, to optimally excite the fundamental or the 1st overtone mode for H_2O sensing. In contrast, the 1653.74 nm beam (L2) is focused onto the base of the tuning fork, specifically on the uncoated quartz surface at the root of the vibrating arm and under an optimized incidence angle in order to maximize the thermoelastic response [44]. The spatial separation of excitation points, together with the inherent frequency-domain isolation of the two modes, should ensure that the signals remain completely independent and unaffected by each other during simultaneous operation.

A commercial gas dilution instrument (MCQ instruments GB100 series) supplies CH_4:N_2 mixtures of controlled concentration to the absorption cell. The inlet flow is regulated using a mass-flow controller (Alicat M-500SCCM-D) and a needle valve, while a vacuum pump (KNF N816.3KT.18) at the outlet maintains stable pressure and flow conditions.

The customized QTF is interfaced with a low-noise trans-impedance amplifier (TA), and the amplified signal is routed to a lock-in amplifier board for second-harmonic (*2 f*) demodulation., with demodulation frequencies set to the fundamental and first-overtone resonance modes, respectively. Both detection channels employed a 12 dB/octave filter slope and all the experiments reported in this work have been performed by fixing the integration time to 1 s. The processed *2 f*, corresponding to photoacoustic and photothermal signals, are recorded and displayed via the data acquisition interface.

3.2. Gas absorption characteristics at 1368.6 nm and 1653.74 nm

To evaluate the performance of the proposed dual-mode system under challenging real-world conditions, atmospheric water vapor (H_2O) and methane (CH_4) were selected as the target gases. This specific gas pair was deliberately chosen to simulate an "extreme dynamic range" scenario typical of environmental monitoring. H2O is a ubiquitous background gas present at massive, percent-level concentrations (typically 1%–5%), whereas CH_4 is a slow-relaxing greenhouse gas found at

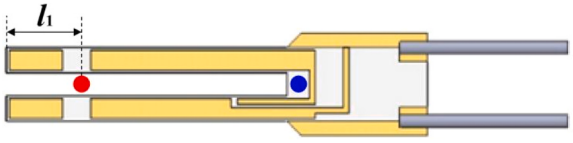

Fig. 3. Laser incidence position to excite the fundamental vibrational mode (red dot) and the 1st overtone vibrational mode (blue dot), l_1= 2.0mm.

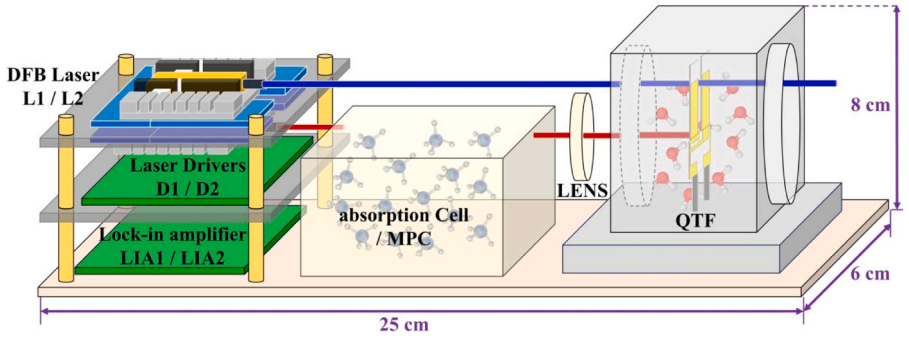

Fig. 2. Main detection modules of the dual spectral multi-gas simultaneous detection system.

trace ppm levels. Additionally, in photoacoustic spectroscopy, H_2O acts as a strong vibrational-translational (V-T) relaxation promoter for CH_4. This physical dependence means that even if the CH_4 concentration remains strictly constant, any fluctuation in ambient water vapor will significantly alter the CH_4 photoacoustic signal amplitude, leading to measurement distortions. Therefore, H_2O must be monitored simultaneously to accurately calibrate the CH_4 measurements in real-world environments. Detecting a weak trace target in the presence of an overwhelming and interfering background is a major bottleneck for conventional sensors. This complex interplay makes this specific gas pair ideal for rigorously validating the system's capacity for crosstalk-free, simultaneous detection across several orders of magnitude. For the experimental implementation, Laser 1 was dedicated to H_2O detection via the photoacoustic excitation. By stabilizing its temperature and current using DL1, the laser was precisely tuned to 1368.6 nm, delivering an output power of 8.8 mW an operating temperature of 23 °C and an injected current of 94.5 mA. This emission wavelength is resonant with a strong H_2O absorption peak at 7306.75 cm^{-1} . Although CH_4 exhibits weak transitions within this spectral region, their line strengths are negligible relative to those of H_2O, ensuring minimal interference from CH_4 during H_2O measurements [43]. Laser 2 dedicated to the photothermal excitation, was tuned to 1653.74 nm using Driver 2 (DL2), providing an output power of 13.8 mW at 32 °C and an injected current of 81.1 mA. In this spectral region, CH_4 exhibits strong absorption features, whereas H_2O absorption lines are significantly weaker and do not compromise the accuracy of CH_4 detection. This deliberate selection of two well-separated absorption bands, coupled with precise wavelength stabilization, effectively suppresses mutual spectral interference and enables reliable, mode-specific detection of H_2O and CH_4.

4. Data analysis of the sensor

4.1. Independence between the two different vibration mode

To verify the independence of the fundamental and first-overtone modes, we first measured the resonance response of the customized QTF under atmospheric pressure. A 150 mV sinusoidal excitation was applied to one electrode of the QTF, while the resulting piezoelectric signal was collected from the opposite electrode. By sweeping the excitation frequency and recording the corresponding amplitude response, the resonance peaks were identified. As shown in Fig. 4, the fundamental resonance frequency was measured to be f_0= 2883.8 Hz, while the first-overtone resonance occurred at f_1= 17839.5 Hz.

Secondly, we experimentally verified the independence of fundamental frequency and 1st overtone mode, as well as the feasibility of simultaneously demodulating photothermal and photoacoustic signals. 5% CH_4 gas mixture was injected into the gas absorption cell and the pressure was stabilized at 686 Torr. At the same time, L2 was modulated

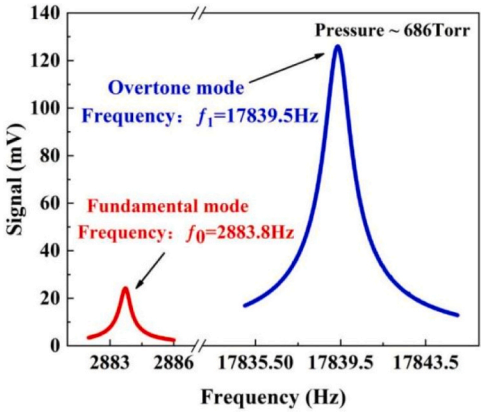

Fig. 4. Resonance spectra of fundamental and 1st overtone mode at 686 Torr.

at half of the fundamental resonance frequency (f_0/2) with an 8 mA modulation depth and a 600 s scan period. The resulting photothermal response at the QTF's overtone frequency was extracted using lock-in amplifier LIA 2. Similarly, 1.6% H_2O was injected into the QTF chamber at the same pressure (686 Torr). L1 was driven with a low-frequency (20 mHz) ramp voltage superimposed on a sinusoidal modulation at f_1/2, with a 2 mA modulation to acquire the 1st overtone wavelength-modulated photoacoustic signal. To demonstrate the capability for simultaneous, interference-free operation, both lasers were then activated concurrently, each at its designated modulation frequency. As shown in Fig. 5(a-b), the QTF produced a clean photothermal signal of 2.5 mV for 5% CH_4 at the fundamental mode and a distinct photoacoustic signal of ~1.64 mV for 1.6% H_2O at the 1st overtone mode. We also inverted the excitation scheme, using the fundamental mode for photoacoustic excitation and the first-overtone mode for photothermal excitation. Fig. 5(c–d) shows the simultaneous signals measured for H_2O (peaks of ~830 μV) and CH_4 (peak of ~5.6 mV). In all operating conditions, the CH_4 spectrum remains unchanged when L2 is switched off, and likewise the H_2O spectrum is unaffected when L1 is disabled. This behavior confirms the complete spectral and modal isolation of the two detection channels.

Based on these observations, we adopted a mode-selective strategy for the subsequent experiments: the first-overtone mode combined with the photothermal effect was used for CH_4 detection, while the fundamental mode combined with the photoacoustic effect was exploited for H_2O detection.

4.2. Optimization of gas pressure

Previous studies have shown that the QEPAS signal exhibits a pressure-dependent maximum because decreasing pressure increases the QTF quality factor while reducing acoustic generation efficiency, leading to an optimal trade-off that maximizes signal amplitude [42]. Likewise, the sensitivity of LITES depends on the pressure of the gas mixture surrounding the QTF. As the pressure decreases, air damping is reduced and the Q-factor of the tuning fork increases, thereby increasing the oscillator accumulation time $\tau = Q/(2\pi f)$. A longer accumulation time enhances the thermoelastic response, resulting in a marked increase in the LITES signal-to-noise ratio at lower pressures [44].

To identify the optimal operating pressure for simultaneous detection, we varied the QTF chamber pressure from 686 Torr to 15 Torr and measured the QTF resonance response. As shown in Fig. 6(a), both the fundamental and first-overtone resonance frequencies increased as the pressure decreased, with a particularly pronounced rise below 100 Torr. At the same time, the Q-factor exhibited a substantial improvement. For example, at 15 Torr for the fundamental mode the Q-factor rises up to 15,270, about 2.5 times higher than its value at 686 Torr, while for the first-overtone mode the Q-factor reach a value of 32,767, representing a ~2.15-fold increase. These trends are expected since reduced pressure enhances QTF resonance sharpness.

Subsequently, simultaneous measurements for a gas mixture of 5% CH_4:N_2 in the absorption cell at a pressure of 686 Torr, while mixtures of 1.6% H_2O:N_2 filled at different pressures the QTF chamber. As shows in Fig. 6(b), the CH_4 photothermal signals increased steadily as the pressure in the QTF chamber decreases, rising from 5.6 mV to ~17.00 mV. In contrast, the H_2O photoacoustic signal exhibited a decreasing trend, dropping from ~830 μV to ~450 μV as pressure inside the QTF chamber was reduced. These opposite pressure-dependent behaviors are fully consistent with previous observations, and demonstrated that the system can operate to simultaneously detect two gases with widely different concentrations using a single customized QTF.

To investigate the sensor system performance, additional measurements were conducted at a fixed pressure of 15 Torr in the QTF chamber. Different CH_4:N_2 mixtures with methane concentrations varying from 50 ppm to 500 ppm were then flushed into the absorption cell, while keeping fixed the pressure to 686 Torr, and the CH_4 photothermal

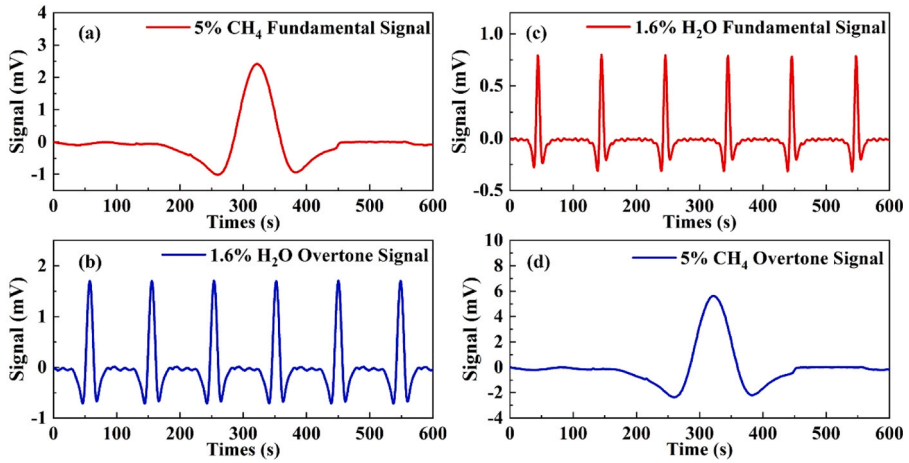

Fig. 5. Independent and simultaneous detection of photoacoustic and photothermal signals using the fundamental and first-overtone modes of the customized QTF. (a) Fundamental-mode photothermal signal generated by 5% CH_4; (b) First-overtone-mode photoacoustic response to 1.6% H_2O; (c) Fundamental-mode photoacoustic signal generated by 1.6% H_2O; (d) First-overtone-mode photothermal response to 5% CH_4.

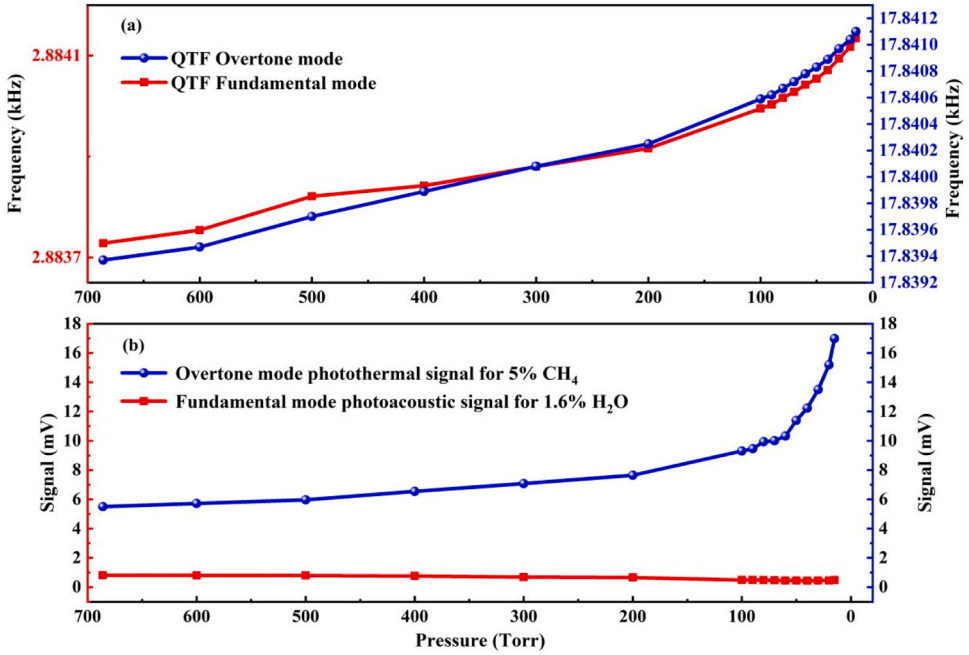

Fig. 6. (a) Resonance frequencies of QTF fundamental and 1st overtone vibrational modes measured at different pressure; (b) Photothermal signal measured for 5% CH_4:N_2 with the QTF operating at the 1st overtone mode and photoacoustic signal of 1.6% H_2O:N_2 while operating the QTF at the fundamental mode, as a function of the surrounding gas pressure.

response was recorded operating the QTF at its 1st overtone mode. The measured signal increases linearly with CH_4 concentration from ~0.2 mV (for 50 ppm) up to ~1.64 mV (for 500 ppm). Linear regression of the concentration-dependent data yielded an R^2 value of 0.998 (Fig. 7 (a)), demonstrating excellent linearity of the CH_4 photothermal response in the investigated methane concentration range.

During the CH_4 detection, the H_2O photoacoustic signal was simultaneously recorded using the fundamental mode. Gas mixture with H_2O concentrations of 0.4%, 0.6%, 0.8%, 1.0%, 1.2%, and 1.6% were introduced into the QTF chamber, keeping fixed the pressure at 15 Torr. The signal increased linearly with water vapor concentration (R^2 = 0.9999), reaching a value of ~450 μV for 1.6% H_2O. The corresponding calibration curve is shown in Fig. 7(b) (red line). Considering the detection bandwidth of 0.833 Hz, 12 dB filter slope and 1 s integration time, the minimum detection limit were calculated to be ~660 ppb for CH_4 and ~30 ppm for H_2O.

To assess the long-term stability of the dual-spectral system, Allan-Werle deviation analysis was performed for both detection channels for a pure N_2 gas sample (Fig. 7(c)-(d)), while keeping the pressure fixed at 686 Torr in the absorption cell and 15 Torr in the QTF chamber. This continuous monitoring lasted for over 1.5 h, providing clear evidence of the system's long-term stability without any observable mode-coupling or resonance drift. The results confirm that sensor noise is dominated by thermal noise up to the averaging time of ~80 s for photothermal and ~200 s for photoacoustic measurements, implying that further sensitivity improvements can be achieved by extending the integration time.

Finally, the system's modularity capability was validated by substituting the LITES absorption cell with a multipass cell providing an optical pathlength ~4.2 m and detecting a 10 ppm CH_4 signal at a pressure of 686 Torr, while simultaneously acquiring the H_2O

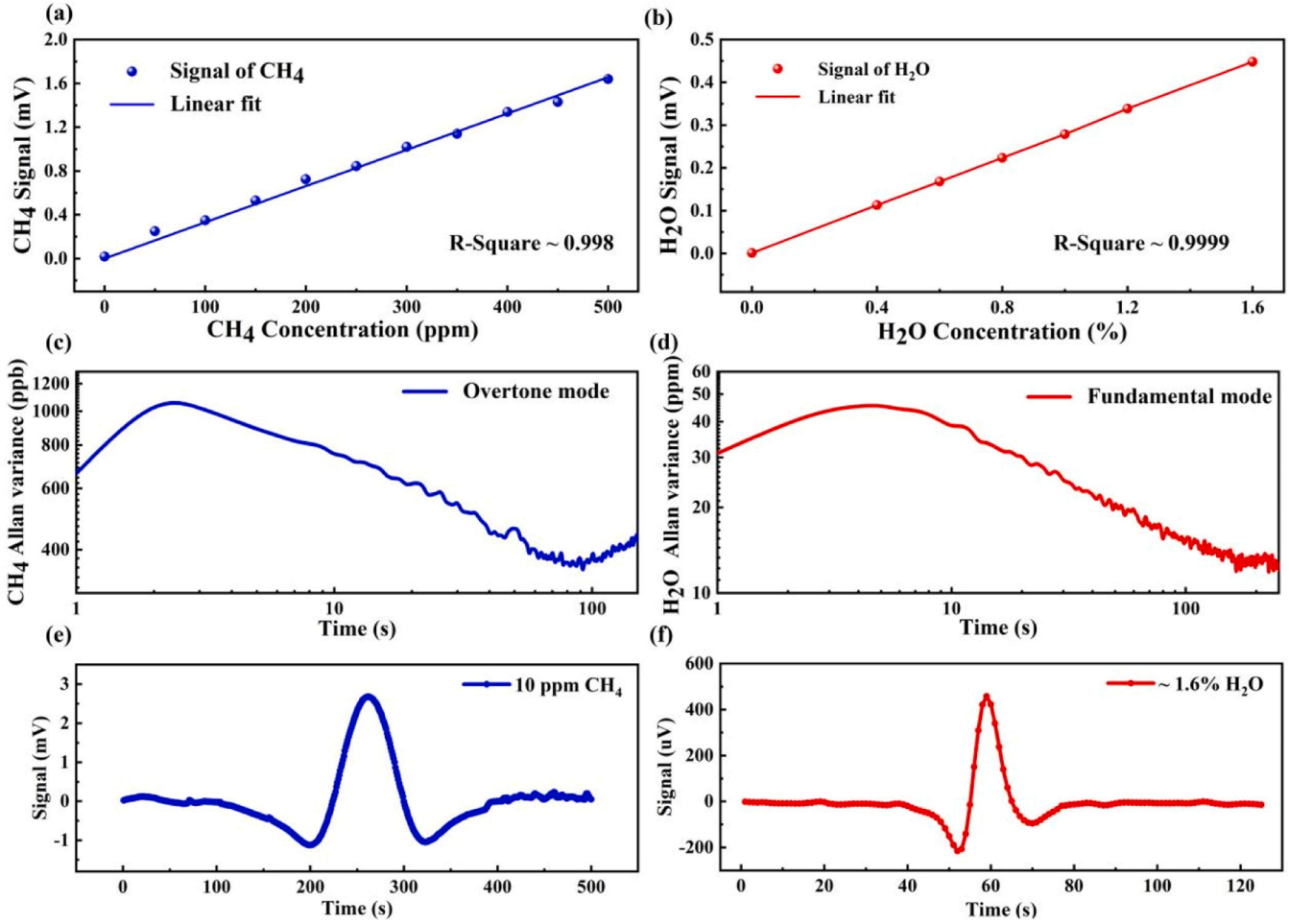

Fig. 7. (a) Photothermal signal (blue dots) measured versus CH_4 concentration. The blue line represents the best linear fit of the data; (b) photoacoustic signal (red dots) measured versus H_2O concentration. The red line represents the best linear fit of the data; (c) Allan-Werle deviations of the photothermal signal measured for pure N_2 samples filling the absorption cell at a pressure of 686 Torr, while L2 wavelength was locked to the CH_4 target absorption line; (d) Allan-Werle deviations of the photoacoustic signal measured for pure N_2 samples filling the QTF chamber at a pressure of 15 Torr, while L2 wavelength was locked to the target H_2O absorption line; (e) 2 *f* photothermal signal measured for 10 ppm CH_4:N_2 at 686 Torr when exploiting a multipass cell with an optical pathlength of ~4.2 m; (f) 2 *f* photoacoustic signal simultaneously measured for 1.6% H_2O: N_2 at 15 Torr filling the QTF chamber.

photoacoustic signal. The measured spectra are shown in Fig. 7(e)–(f), with a peak value measured for methane of ~2.75 mV, demonstrating the modularity of the proposed simultaneous dual-gas detection system.

5. Conclusions

In this work, we demonstrated a dual-spectral multi-gas detection system that combines QEPAS and LITES within a single customized quartz tuning fork. By simultaneously exciting the fundamental and first-overtone resonance modes, the proposed architecture enables intrinsic frequency-domain separation of photoacoustic and photothermal responses, allowing truly simultaneous, crosstalk-free detection of gases that differ in concentration by several orders of magnitude. Using H_2O at percent-level and CH_4 at ppm-level as representative targets, we achieved excellent linearity, high sensitivity, and robust long-term stability. The system also allow to easily exchange the absorption cell type in the LITES module, as demonstrated through 10-ppm methane detection exploiting a multipass cell with an optical pathlength of ~4.2 m.

Pressure-dependent studies confirmed that the two modes behave independently and can be optimized separately, enabling efficient signal extraction for both high- and low-concentration gases. The simplified optical configuration, single-resonator design, and strong resistance to spectral and modal interference collectively establish this dual-mode approach as a versatile and scalable platform for wide-dynamic-range gas sensing.

In future real-world deployment, a sequential flow architecture will be developed. The gas mixture will, for example, first enter the LITES multi-pass absorption cell and subsequently flow into the QEPAS QTF chamber. Since QEPAS and LITES require different optimal operating pressures, a proportional micro-metering valve (or a differential pressure controller) will be implemented in the gas line connecting the two chambers. This configuration will allow employing a single continuous sample intake while actively maintaining the independent optimal pressures.

Overall, the results bridge the performance gap between traditional single-mode QEPAS or LITES systems and the requirements of modern multi-component monitoring in complex or open-path environments. Future developments will include extending the approach to additional molecular species, refining QTF geometries to enhance robustness in harsh environments, and exploring multiplexed operation via higher-order overtone modes. These advancements will further expand the applicability of the technique to challenging scenarios such as industrial emission monitoring, high-temperature process control, and atmospheric sensing.

CRediT authorship contribution statement

Hongpeng Wu: Writing – review & editing, Supervision, Resources, Methodology, Data curation, Conceptualization. **Vincenzo Spagnolo:** Writing – review & editing, Supervision, Methodology, Conceptualization. **Lei Dong:** Writing – review & editing, Supervision, Methodology, Funding acquisition, Conceptualization. **Pietro Patimisco:** Writing – review & editing, Methodology, Conceptualization. **Angelo Sampaolo:** Writing – review & editing, Methodology, Conceptualization. **Xiaowen Shen:** Writing – original draft, Methodology, Investigation, Conceptualization. **Chaofeng Sun:** Methodology, Investigation, Data curation, Conceptualization.

Declaration of Competing Interest

The authors declare that they have no known competing financial interests or personal relationships that could have appeared to influence the work reported in this paper.

Acknowledgments

This project was supported by the National Science and Technology Major Project of China (Grant No. 2025ZD1200704); The National Natural Science Foundation of China (NSFC) (Nos. 62475137, 62235010, 62502163, 62501370); Shanxi Provincial Special Fund for Scientific and Technological Cooperation and Exchange (202404041101022, 202304041101019); Fundamental Research Program of Shanxi Province, China (No. 202403021212183, 202303021222034); The Scientific and Technological Innovation Programs of Higher Education Institutions in Shanxi Province of China (2024L014); The National Engineering Research Center of UHV Technology and New Electrical Equipment Basis (Grant No. NERCUHE-2024-KF-12). Authors from Polysense Lab acknowledge funding from Project PNC 0000001 D3–4-Health—Digital Driven Diagnostics, prognostics and therapeutics for sustainable Health care (CUP: B83C22006120001); MUR – Dipartimenti di Eccellenza 2023–2027 – Quantum Sensing and Modelling for One-Health (QuaSiModO) and THORLABS GmbH within the PolySenSe joint research laboratory.

Data availability

Data will be made available on request.

References

[1] C.B.S. Dubeux, E.L.La Rovere, Local perspectives in the control of greenhouse gas emissions–the case of Rio de Janeiro, Cities 24 (2007) 353–364, https://doi.org/10.1016/j.cities.2007.01.012.
[2] J. Hodgkinson, R.P. Tatam, Optical gas sensing: a review, Meas. Sci. Technol. 24 (2012) 012004, https://doi.org/10.1088/0957-0233/24/1/012004.
[3] X. Liu, S. Cheng, H. Liu, S. Hu, D. Zhang, H. Ning, A survey on gas sensing technology, Sensors 12 (2012) 9635–9665, https://doi.org/10.3390/s120709635.
[4] D. Kohl, Function and applications of gas sensors, J. Phys. D Appl. Phys. 34 (2001) R125, https://doi.org/10.1088/0022-3727/34/19/201.
[5] A. Sampaolo, P. Patimisco, M. Giglio, A. Zifarelli, H. Wu, L. Dong, V. Spagnolo, Quartz-enhanced photoacoustic spectroscopy for multi-gas detection: a review, Anal. Chim. Acta 1202 (2022) 338894, https://doi.org/10.1016/j.aca.2021.338894.
[6] A.K. Farquhar, G.S. Henshaw, D.E. Williams, Understanding and correcting unwanted influences on the signal from electrochemical gas sensors, ACS Sens. 6 (2021) 1295–1304, https://doi.org/10.1021/acssensors.0c02589.
[7] P. Liu, J. Li, C. Xia, Y. He, S. Wang, Interference study of multiple gases on electrochemical sensors in flue, Metrol. Sci. Technol. 67 (62–67) (2023) 52, https://doi.org/10.12338/j.issn.2096-9015.2023.0221.
[8] M.Z. Abidin, A. Asmat, M.N. Hamidon, Temperature drift identification in semiconductor gas sensors, 2014 IEEE Conf. Syst. Process Control (ICSPC 2014) (2014) 63–67, https://doi.org/10.1109/SPC.2014.7086231.
[9] C. Liu, X.C. Zhou, G. Li, J. Su, L. Tang, Q. Liu, X. Han, S. Lv, Z. Mu, Y. Sun, S. Yuan, F. Gao, J. Zuo, S. Li, M. Ding, Ligand spin immobilization in metal-organic frameworks enables high-performance chemispintronic detection of radical gas molecules, Sci. Adv. 11 (2025) eadq3554, https://doi.org/10.1126/sciadv.adq3554.
[10] X. Fang, H. Wang, H. Xu, M. Huang, X. Liu, Identification and detection of multi-component trace gases based on near-infrared TDLAS technology based on SVM, Spectrosc. Spect. Anal. 44 (2024) 2909–2915.
[11] J. Sun, J. Chang, C. Wang, J. Shao, Tunable diode laser absorption spectroscopy for detection of multi-component gas: a review, Appl. Spectrosc. Rev. 59 (2024) 1086–1107, https://doi.org/10.1080/05704928.2024.2302608.
[12] S. Schilt, L. Thevenaz, P. Robert, Wavelength modulation spectroscopy: combined frequency and intensity laser modulation, Appl. Opt. 42 (2003) 6728–6738, https://doi.org/10.1364/AO.42.006728.
[13] X. Yin, Q. Hu, X. Yang, K. Xu, Y. Liang, J. Hou, A. Sampaolo, P. Patimisco, V. Spagnolo, D. Zhang, Z. Liu, H. Xu, H. Wu, Ppb-level HF sensor in GeF_4 gas matrices with a 76 m TDLAS cell, Sens. Actuators B Chem. (2025) 139141, https://doi.org/10.1016/j.snb.2025.139141.
[14] H. Fuchs, W.P. Dubé, B.M. Lerner, N.L. Wagner, E.J. Williams, S.S. Brown, A sensitive and versatile detector for atmospheric NO_2 and NO_x based on blue diode laser cavity ring-down spectroscopy, Environ. Sci. Technol. 43 (2009) 7831–7836, https://doi.org/10.1021/es902067h.
[15] K. Zheng, C. Zheng, N. Ma, Z. Liu, Y. Yang, Y. Zhang, Y. Wang, F.K. Tittel, Near-infrared broadband cavity-enhanced spectroscopic multigas sensor using a 1650 nm light emitting diode, ACS Sens 4 (2019) 1899–1908, https://doi.org/10.1021/acssensors.9b00788.
[16] X. Liu, H. Wu, L. Dong, Methodology and applications of acousto-electric analogy in photoacoustic cell design for trace gas analysis, Photoacoustics 30 (2023) 100475, https://doi.org/10.1016/j.pacs.2023.100475.
[17] X. Yang, B. Li, X. Geng, T. Zhao, Q. Yu, J. Hou, D. Zhang, Y. Liang, K. Xu, H. Wu, X. Yin, Ppb-level formaldehyde sensor utilizing a compact 3D-printed differential photoacoustic cell and a 320 nm UV Laser, Photoacoustics 46 (2025) 100780, https://doi.org/10.1016/j.pacs.2025.100780.
[18] Y. Wang, J. Wang, G. Wang, J. Dai, R. Cui, C. Feng, M. Olivieri, A. Sampaolo, P. Patimisco, V. Spagnolo, L. Dong, H. Wu, Investigation of the role of photoacoustic phase in N_2O(v3) vibrational relaxation rate determination, Sens. Actuators B Chem. 450 (2026) 139207, https://doi.org/10.1016/j.snb.2025.139207.
[19] G. Wu, L. Zhang, T. Gao, Z. Gong, Y. Guan, J. Xing, M. Zhang, W. Peng, L. Mei, Highly sensitive non-invasive hemispherical fiber optic photoacoustic sensor utilizing dual radial and angular resonant modes for simultaneous multi-gas detection, Anal. Chem. 98 (3) (2026) 2569–2578, https://doi.org/10.1021/acs.analchem.5c07830.
[20] G. Wu, Y. Guan, X. Li, Z. Gong, P. Wei, L. Mei, PET-cantilever-enhanced fiber-optic photoacoustic spectroscopy for rapid sub-ppm methane detection, Anal. Chem. 97 (28) (2025) 15510–15515, https://doi.org/10.1021/acs.analchem.5c03433.
[21] G. Wu, L. Zhang, Y. Guan, Z. Gong, T. Gao, J. Xing, M. Zhang, W. Peng, L. Mei, Dual-enhanced fiber-optic photoacoustic spectroscopy via asymmetric cavity coupling and cantilever amplification for sub-ppb C_2H_2 detection, Sens. Actuators B Chem. 458 (2026) 139827, https://doi.org/10.1016/j.snb.2026.139827.
[22] Y. Ma, Review of recent advances in QEPAS-based trace gas sensing, Appl. Sci. 8 (2018) 1822, https://doi.org/10.3390/app8101822.
[23] A.A. Kosterev, Y.A. Bakhirkin, R.F. Curl, F.K. Tittel, Quartz-enhanced photoacoustic spectroscopy, Opt. Lett. 27 (2002) 1902–1904, https://doi.org/10.1364/OL.27.001902.
[24] A. Sampaolo, P. Patimisco, L. Dong, A. Geras, G. Scamarcio, T. Starecki, F.K. Tittel, V. Spagnolo, Quartz-enhanced photoacoustic spectroscopy exploiting tuning fork overtone modes, Appl. Phys. Lett. 107 (23) (2015), https://doi.org/10.1063/1.4937002.
[25] H. Wu, X. Yin, L. Dong, K. Pei, A. Sampaolo, P. Patimisco, H. Zheng, W. Ma, L. Zhang, W. Yin, L. Xiao, V. Spagnolo, S. Jia, F.K. Tittel, Simultaneous dual-gas QEPAS detection based on a fundamental and overtone combined vibration of quartz tuning fork, Appl. Phys. Lett. 110 (2017) 12, https://doi.org/10.1063/1.4979085.
[26] A. Elefante, M. Giglio, A. Sampaolo, G. Menduni, P. Patimisco, V.M.N. Passaro, H. Wu, H. Rossmadl, V. Mackowiak, A. Cable, F.K. Tittel, L. Dong, V. Spagnolo, Dual-gas quartz-enhanced photoacoustic sensor for simultaneous detection of methane/nitrous oxide and water vapor, Anal. Chem. 91 (2019) 12866–12873, https://doi.org/10.1021/acs.analchem.9b02709.
[27] A. Sampaolo, P. Patimisco, M. Giglio, A. Elefante, V. Passaro, F.K. Tittel, V. Spagnolo, Simultaneous dual gas QEPAS sensing of water and methane/nitrous oxide, in: Quantum Sensing and Nano Electronics and Photonics XVI, 10926, SPIE, 2019, pp. 300–307, https://doi.org/10.1117/12.2507922.
[28] R. De. Palo, A. Volpe, P. Patimisco, A. Zifarelli, A. Sampaolo, A. Ancona, H. Wu, V. Spagnolo, Femtosecond laser fabrication of black quartz for infrared photodetection applications, Light. Adv. Manuf. 6 (1) (2025) 1–11, https://doi.org/10.37188/lam.2025.026.
[29] J. Wang, H. Wu, A. Sampaolo, P. Patimisco, V. Spagnolo, S. Jia, L. Dong, Quartz-enhanced multiheterodyne resonant photoacoustic spectroscopy, Light Sci. Appl. 13 (2024) 77, https://doi.org/10.1038/s41377-024-01425-1.
[30] Z. Wang, Q. Wang, H. Zhang, S. Borri, I. Galli, A. Sampaolo, P. Patimisco, V. Spagnolo, P. Natale, W. Ren, Doubly resonant sub-ppt photoacoustic gas detection with eight decades dynamic range, Photoacoustics 27 (2022) 100387, https://doi.org/10.1016/j.pacs.2022.100387.
[31] S. Das, M. Pal, Review-Non-invasive monitoring of human health by exhaled breath analysis: a comprehensive review, J. Electrochem. Soc. 167 (2020) 037562, https://doi.org/10.1149/1945-7111/ab67a6.
[32] C.A. Grimes, K.G. Ong, O.K. Varghese, X. Yang, G. Mor, M. Paulose, E.C. Dickey, C. Ruan, M.V. Pishko, J.W. Kendig, A.J. Mason, A sentinel sensor network for hydrogen sensing, Sensors 3 (2003) 69–82, https://doi.org/10.3390/s30300069.

[33] Y. Ma, Y. He, Y. Tong, X. Yu, F.K. Tittel, Quartz-tuning-fork enhanced photothermal spectroscopy for ultra-high sensitive trace gas detection, Opt. Express 26 (2018) 32103–32110, https://doi.org/10.1364/OE.26.032103.
[34] S. Qiao, Z. Lang, Y. He, X. Zhi, Y. Ma, Calibration-free measurement of absolute gas concentration and temperature via light-induced thermoelastic spectroscopy, Adv. Photonics 7 (2025) 066007, https://doi.org/10.1117/1.AP.7.6.066007.
[35] J. Dai, C. Wang, P. Liu, L. Huang, Y. Li, C. Lou, Y. Ma, Sensitive light-induced thermoelastic spectroscopy-based oxygen sensor with a perovskite-modified quartz tuning fork, IEEE Sens. J. 23 (19) (2023) 22380–22388, https://doi.org/10.1109/JSEN.2023.3304654.
[36] H. Fan, M. Hu, H. Zhang, D. Zhang, Q. Wang, Cavity-enhanced beat frequency light-induced thermoelastic spectroscopy using differential-frequency demodulation, ACS Sens. 10 (2025) 9068–9076, https://doi.org/10.1021/acssensors.5c03615.
[37] Y. Hu, S. Qiao, Y. He, Z. Lang, Y. Ma, Quartz-enhanced photoacoustic-photothermal spectroscopy for trace gas sensing, Opt. Express 29 (2021) 5121–5127, https://doi.org/10.1016/j.fuel.2020.118118.
[38] S. Qiao, Y. He, Y. Ma, Trace gas sensing based on single-quartz-enhanced photoacoustic-photothermal dual spectroscopy, Opt. Lett. 46 (2021) 2449–2452, https://doi.org/10.1364/OL.423801.
[39] R. Cui, H. Wu, F.K. Tittel, V. Spagnolo, W. Chen, L. Dong, Folded-optics-based quartz-enhanced photoacoustic and photothermal hybrid spectroscopy, Photoacoustics 35 (2024) 100580, https://doi.org/10.1016/j.pacs.2023.100580.
[40] Changchun Institute of Optics, Fine Mechanics and Physics, CAS, CIOMP. ⟨http://www.ciomp.ac.cn/xwdt/zhxw/202501/t20250114_7517723.html⟩ (accessed 14 January 2025).
[41] J.M. Friedt, E. Carry, Introduction to the quartz tuning fork, Am. J. Phys. 75 (2007) 415–422, https://doi.org/10.1119/1.2711826.
[42] F.K. Tittel, A. Sampaolo, P. Patimisco, L. Dong, A. Geras, T. Stareki, V. Spagnolo, Analysis of overtone flexural modes operation in quartz-enhanced photoacoustic spectroscopy, Opt. Express 24 (2016) A682–A692, https://doi.org/10.1364/OE.24.00A682.
[43] HITRAN Database, HITRAN, ⟨https://hitran.org⟩.
[44] S.D. Russo, A. Zifarelli, P. Patimisco, A. Sampaolo, T. Wei, H. Wu, L. Dong, V. Spagnolo, Light-induced thermo-elastic effect in quartz tuning forks exploited as a photodetector in gas absorption spectroscopy, Opt. Express 28 (2020) 19074–19084, https://doi.org/10.1364/OE.393292.

Xiaowen Shen is now pursuing a Ph.D. degree in atomic and molecular physics at both the Institute of Laser Spectroscopy of Shanxi University, China and Polysense Lab at the Technical University of Bari, Italy. Her research is focused on the development of gas sensors, photoacoustic spectroscopy, photothermal spectroscopy and laser spectroscopy techniques.

Chaofeng Sun is now pursuing a Ph.D. degree in atomic and molecular physics in the Institute of Laser Spectroscopy of Shanxi University, China. His research is focused on the development of photoacoustic spectroscopy, photothermal spectroscopy and laser spectroscopy techniques.

Pietro Patimisco obtained the Master degree in Physics (cum laude) in 2009 and the Ph.D. Degree in Physics in 2013 from the University of Bari. Since 2023, he is Associate professor at the University of Bari. He was a visiting scientist in the Laser Science Group at Rice University in 2013 and 2014. Dr. Patimisco's scientific activity addressed both micro-probe optical characterization of semiconductor optoelectronic devices and optoacoustic gas sensors. Recently, his research activities included the study and applications of trace-gas sensors, such as quartz-enhanced photoacoustic spectroscopy and cavity enhanced absorption spectroscopy in the mid infrared and terahertz spectral region. His research activity is documented by more than 180 Scopus publications and 6 filed patents (more than 7100 citations, h-index 52).

Angelo Sampaolo obtained his Master degree in Physics in 2013 and the Ph.D. Degree in Physics in 2017 from University of Bari. He was an associate researcher in the Laser Science Group at Rice University from 2014 to 2016 and associate researcher at Shanxi University since 2018. Starting from December 2024, he is Associate Professor at Polytechnic of Bari. His research activity has included the study of the thermal properties of heterostructured devices via Raman spectroscopy. Most recently, his research interest has focused on the development of innovative techniques in trace gas sensing, based on Quartz-Enhanced Photoacoustic Spectroscopy and covering the full spectral range from near-IR to THz. His research activity is documented by more than 180 Scopus publications and 6 filed patents (more than 6100 citations, h-index 50)

Vincenzo Spagnolo obtained the Ph.D. in physics in 1994 from University of Bari. Since 2004, he works at the Technical University of Bari, formerly as assistant and associate professor and, starting from 2018, as full Professor of Physics. Since 2025, he director of the PhD School in Physics of the University of Bari. He is the director of the joint research lab Polysense between Technical University of Bari and THORLABS GmbH, fellow member of SPIE and senior member of OSA. His research interests include optoacoustic gas sensing and spectroscopic techniques for real-time monitoring. His research activity is documented by more than 330 publications and six filed patents. He has given more than 70 invited presentations at international conferences and workshops.

Lei Dong received his Ph.D. degree in optics from Shanxi University, China, in 2007. From June, 2008 to December, 2011, he worked as a post-doctoral fellow in the Electrical and Computer Engineering Department and Rice Quantum Institute, Rice University, Houston, USA. Currently he is a professor in the Institute of Laser Spectroscopy of Shanxi University. His research activities research activities are focused on research and development in laser spectroscopy, in particular photoacoustic spectroscopy applied to sensitive, selective and real-time trace gas detection, and laser applications in environmental monitoring, chemical analysis, industrial process control, and medical diagnostics. He has published more than 100 peer reviewed papers with $>$ 2200 positive citations.

Hongpeng Wu received his Ph.D. degree in atomic and molecular physics from Shanxi University, China, in 2017. From 2015–2016, he studied as a joint Ph.D. student in the electrical and computer engineering department and rice quantum institute, Rice University, Houston, USA. Currently he is a professor in the Institute of Laser Spectroscopy of Shanxi University. His research interests include optical sensors and laser spectroscopy techniques.